Design and construction of a silver(I)-loaded cellulose-based wound dressing: trackable and sustained release of silver for controlled therapeutic delivery to wound sites

T. R. deBoer[1], **I. Chakraborty**[1], and **P. K. Mascharak**[1]

[1]Department of Chemistry and Biochemistry, University of California, Santa Cruz, 1156 High Street, Santa Cruz, CA 95064, USA

Abstract

Although application of silver nitrate and silver sulfadiazine have been shown to be effective in thwarting infections at burn sites, optimization of the delivery of bioactive silver (Ag^+) remains as an obstacle due to rapid precipitation and/or insolubility of the silver sources. To circumvent these shortcomings, we have designed a silver(I) complex $[Ag(ImD)_2]ClO_4$ (ImD = dansyl imidazole) that effectively increases the bioavailability of Ag^+ and exhibits MIC values of 2.3 and 4.7 μg/mL against *E. coli* and *S. aureus*, respectively. This fluorescent silver complex has been incorporated within a robust hydrogel derived from carboxymethyl cellulose that allows slow release of silver. A complete occlusive dressing has finally been constructed with the $Ag(ImD)_{CMC}$ (1 % Ag loaded) pad sealed between a sterile mesh gauze (as bottom layer) and a rayon-based surgical tape (as the top layer). Such construction has afforded a dressing that displays sustained delivery of silver onto a skin and soft tissue infection model and causes effective eradication of bacterial loads within 24 h. The transfer of the bioactive silver complex is readily visualized by the observed fluorescence that overlays precisely with the kill zone. The latter feature introduces a unique feature of therapeutic trackability to this silver-donating occlusive dressing.

1 Introduction

The nobel metal silver represents an ancient antiseptic therapy option that was quickly neglected with the advent of antibiotics during the 1930s and 1940s [1]. However, resurgence of silver-based therapeutics as bactericidal options has been evident given the prevalence of antibacterial resistance and the appearance of *super bugs* [2, 3]. Ionized silver (Ag^+) is the bioactive form of silver that is capable of reacting with a broad spectrum of biomolecules, including DNA, amino acid residues, and compounds with sulfhydryl groups. Ag^+ elicits cytotoxic effects in microorganisms by inducing physical cell wall damage, enhancing membrane permeability, disrupting ATP production and DNA replication, and generating reactive oxygen species (ROS) [4, 5].

Because oral consumption of metals in general can yield detrimental effects, silver has commonly been applied topically to treat infections in superficial wounds. Silver-based therapies have been used to treat acute and chronic wounds in the form of silver-impregnated wound dressings and Ag^+ salt solutions [1, 6]. While the antimicrobial efficacy of Ag^+ has been well established, optimization of Ag^+ delivery at wounds sites remains as an obstacle. Common topical burn wound therapy using silver salt $AgNO_3$ requires wound site irrigation with a 1 % $AgNO_3$ solution every 2 h (12 times daily), a process highly undesirable for both patients and healthcare professionals. Unfortunately, frequent therapeutic applications with silver salt solutions are required because they lack residual activity capabilities [6].

To address these shortcomings, silver-impregnated wound dressings have become an attractive option because they offer extended residual therapeutic activity, decreased wound site exposure, and require significantly less frequent manipulation of the wound site [7]. All of these features collectively contribute to the possibility of increasing patient compliance and reducing the time required for wound healing. There are several silver *carrier* dressings currently on the market, constructed from dense polymeric frames that are designed to maintain optimal wound moisture levels in addition to releasing therapeutic levels of silver [8]. Silver-based therapeutics commonly loaded into carrier wound dressings range from silver nanoparticles (Ag-NP) to free Ag^+. Although incorporation of ionic silver into a carrier material has the potential of affording the highest level of therapeutic capacity, complication arising from its reactivity towards non-specific proteins and electrolytes can result in its rapid consumption and diminished therapeutic efficacy. Nevertheless, the choice and design of the delivery frame of a silver-based wound dressing can be modulated to further optimize the rate of Ag^+ release to the wound sites, a level of control unattainable with silver salt solutions or silver-based creams.

In addition to impeding the bacterial load at open wounds sites, dressings can contribute to the global wound healing process. This dynamic process requires optimal moisture balance for proper re-epithelialization and tissue remodeling (two of the four wound healing stages) [9–11]. Low moisture environments commonly give rise to scab formation that inhibits both stages by creating a mechanical barrier. Scabs block translation of epidermal cells towards the surface and force them down into deeper layers of the tissue extending the healing time and giving rise to abnormal tissue architecture and scarring [12]. Hydrocolloid materials are one example of occlusive dressings that are capable of absorbing wound exudate and maintaining proper levels of moisture in wounds. Cellulose-based polymers represent a large class of hydrocolloid dressings that display effective swelling properties easily modulated with chemical derivatization. Although it was initially believed that occlusive dressings could inhibit oxygenation and facilitate bacterial growth at wound sites, Winter and coworkers demonstrated decreased healing times with application of occlusive dressings to non-ischemic wounds [13]. Application of hydrocolloid-based dressings not only provides optimal wound moisture levels but also contributes to improved patient comfort because as moisture penetrates the dressing, the surface becomes gelatinous and minimizes resistance during cleaning and replacement of expended dressings.

The potential of occlusive silver-loaded wound dressings in the management of wound healing and infection is evident given the exponential growth in the number of publications

highlighting the design of silver-based therapeutics and wound dressings over the last decade. Still, the vast majority of silver-loaded wound dressings available on the market incorporate traditional silver sources such as $AgNO_3$ and Ag-sulfadiazine (Ag-SD) or Ag-NPs [5]. In the present work, we report the design and synthesis of a silver-loaded dressing that has been constructed in three layers with a hydrophobic rayon-based surgical tape on the top, a prefabricated silver(I)-loaded hydrocolloid pad in the middle, and a sterile mesh gauze at the bottom. The hydrocolloid pad features a unique *trackable* drug delivery modality through the incorporation of a blue-green fluorescent silver (I) complex $[Ag(ImD)_2]ClO_4$ (**1**, λ_{em} = 600 nm) into the carrier sodium carboxymethyl cellulose (Na-CMC) frame ($Ag(ImD)_{CMC}$ hereafter). The luminescent properties of the silver complex allows for quantitative determination of **1** release rates from the hydrocolloid pad by both fluorescence and electronic absorption spectroscopy. Further, the effective delivery of **1** from the occlusive dressing to a wound site can be readily established in solid-phase leaching studies, where movement of **1** out the Na-CMC frame onto an agar surface is visually tracked using a hand-held ultraviolet (UV) wand. The results discussed bellow demonstrate the potential of fluorescent silver(I) complexes as tunable components of silver-loaded wound dressings that can be tailored to impart trackable release of silver therapeutics to wound sites.

2 Materials and methods

2.1 Synthesis of [Ag(ImD)₂]ClO₄ (1)

A solution of 27 mg (100 mmol) of $AgClO_4$ in dry acetonitrile (ACN) was added drop-wise to a rapidly stirred solution of 130 mg (200 mmol) of dansyl imidazole (ImD) in the same solvent (ACN) and the mixture was allowed to stir for 3 h. A dark orange microcrystalline solid formed when this reaction mixture was concentrated to one-half the original volume and stored at 4 °C for 24 h. The silver salt was finally recrystallized by allowing diffusion of diethyl ether vapor into the solution of the metal complex in dry acetonitrile at 4 °C. At the end of 72 h, X-ray quality orange needles were isolated and structurally analyzed by single crystal X-ray diffraction studies. ^1H NMR spectrum in $CDCl_3$ (Varian Unity, 500 MHz): 8.70 (d), 8.44 (m), 8.26 (d), 7.69 (t), 7.63 (t), 7.22 (d), 7.18 (s), 7.00 (s), 2.87 (s). IR (KBr disk): 636 cm^{-1}, 786 cm^{-1} (s), 1092 cm^{-1}, 1375 cm^{-1}, and 1462 cm^{-1}. Electronic absorption spectrum (Carey 5000 spectrophotometer): λ_{max} = 360 nm (ε = 7,735 M^{-1} cm^{-1}).

2.2 X-ray diffraction data

Data were collected on a Bruker APEX II single crystal X-ray diffractometer with graphite monochromated Mo Kα radiation (k = 0.71073 Å) by the x-scan technique in the range 3 ≤ 2h ≤ 50. All data were corrected for Lorentz-polarization and absorption. The metal atoms were located from Patterson maps and the rest of the non-hydrogen atoms emerged from successive Fourier syntheses. The structures were then refined by a full-matrix least squares procedure on F^2. All non-hydrogen atoms were refined anisotropically. All hydrogen atoms were included in calculated positions. The absorption corrections are done using SADABS. Calculations were performed using the SHELXTL™ (V 6.14) program package. The summary of crystal data and structure refinement parameters, and Table for selected bond distances and angles are both included in the Supporting Information.

2.3 [Ag(ImD)$_2$]ClO$_4$ photostability and biocompatibility assay

A solution of 10 mg of **1** into 0.7 mL of CD$_3$CN was prepared and its ^{1}H NMR spectrum was acquired immediately (defined as time 0). The sample was then properly sealed to minimize solvent evaporation and left in ambient light. Subsequent ^{1}H NMR spectra were recorded at 8, 12 and 24 h. Exposure intervals are defined strictly as the time of light exposure and do not include acquisition time. For qualitative comparison, a solution of AgNO$_3$ was also prepared by dissolving 5 mg of AgNO$_3$ in 0.7 mL of CD$_3$CN. This control sample was also sealed and set directly adjacent to the solution containing **1** under ambient light for equivalent time exposure. No photodecomposition was evident in the solution of **1** within 24 h. In contrast, the AgNO$_3$ solution turned dark purple brown within 1 h. A second stability experiment was also performed with a solution of **1** in minimal recovery diluent (MRD) to establish the compatibility of the silver complex in biological media. The integrity of the complex was checked by monitoring its emission band at 500 nm (Varian Cary Eclipse fluorimeter) for 24 h.

2.4 Preparation of Ag(ImD)$_{CMC}$ (1 % Ag loaded) wound dressing

Assembly of the occlusive wound dressing first required the preparation of the (**1**)-loaded CMC pad. The hydro-colloid gel was prepared by adding 0.53 g of NaCMC (3.5 % w/v) to 0.75 g of 2000 MW polyethylene glycol (PEG, 5 % w/v) in a 50 mL beaker. To this mixture, a batch of 13.5 mL of deionized MilliQ water was added drop wise. The slurry was allowed to stir until the solid was completely dissolved into water. Next, a solution of 5 mg of **1** in 0.95 mL of ACN was added drop wise under mild stirring velocity. The final solution was transferred into a sterile culture dish (60 mm), weighed, and placed into a desiccator to dry. Each pad was dried to 30 ± 1 % its original weight (75 % solvent loss by weight) to assure uniformity from batch to batch, calculated by the following equation: % solvent loss = (*initial* weight of Ag(ImD)$_{CMC}$ gel (W$_i$) − weight of dried Ag(ImD)$_{CMC}$ (W$_f$))/W$_i$.

The occlusive dressings could be prepared in variable dimensions and shapes. In the present work, circular Ag(ImD)$_{CMC}$ discs (1 cm diameter) were layered between a 1.5 cm sterile ultra-soft latex-free gauze square and a 1.5 cm rayon-based Durapore ™ surgical tape and the constructs were employed for antibacterial studies. The Ag(ImD)$_{CMC}$ discs were first placed onto a pre-cut gauze surface and then the paired surgical tape piece was gently placed on top of the gel pad. The assembly was then sealed by applying gentle pressure to edges of the adhesive tape down onto the gauze surface. All Ag(ImD)$_{CMC}$ discs were weighed prior to being incorporated into the dressing construct. The average disc weight was determined to be 75.6 mg and only discs weighing within the standard deviation were used.

2.5 Release of 1 from Ag(ImD)$_{CMC}$ pad into aqueous media

The rates of release of **1** from the Ag(ImD)$_{CMC}$ pads were quantified by absorption and fluorescence spectroscopy. Maximum recovery diluent (MRD, 1 g/L Peptone, 8.5 g NaCl, 0.01 M Phosphate buffer, pH 7.0) was selected as the solvent for all studies in attempts to provide milieu similar to media required for antibacterial studies. In each study, pre-weighed circular Ag(ImD)$_{CMC}$ discs (1 cm diameter) were added to quartz cuvettes (10 mm Starna cuvette) containing 3 mL of MRD. In both absorption and fluorescence spectroscopy studies, the cuvettes were kept stationary in the respective sample holders and spectral

readings were taken every 20 min for 24 h. The leaching profile of Ag(ImD)$_{CMC}$ was established by converting the observed change in absorbance at 360 nm ($\varepsilon = 7735$ M^{-1} cm^{-1}) to concentration by Beer's Law and plotting these values against the corresponding time. Leaching of **1** from the hydrocolloid pad was also qualitatively monitored with the aid of fluorescence spectroscopy. Each experiment was run in triplicate unless otherwise noted.

2.6 Release of 1 from Ag(ImD)$_{CMC}$ pad onto agar surface

Agar plates (5 % Agar) were prepared in 100 mm culture dishes, and to each plate 3 pre-weighed Ag(ImD)$_{CMC}$ discs (1 cm diameter) were placed onto the agar surface. MRD was added to the discs to initiate gelation of the disc and facilitate movement of **1** out of the carboxymethyl cellulose frame. These plates were kept stationary and allowed to incubate for 24 h. The translocation of **1** from Ag(ImD)$_{CMC}$ discs was visually evaluated at 2, 4, 6, 8, 12, and 24 h time points using a UV table top lamp (UVP™ UV transilluminator, broad range 200–325 nm). At each time point, dressings were removed and the relative luminescence of the agar surface was noted photographically. Studies were conducted with 1 and 0.5 % Ag(ImD)$_{CMC}$ to determine changes in the rate of leaching of **1** from the hydrocolloid gel pad as a function of therapeutic loading.

2.7 Minimal inhibitory concentration (MIC) assay

Gram-positive and Gram-negative bacteria (*E. coli* and *S. aureus*, respectively) were grown up to 1.0×10^8 CFU mL from single colony growths in Müller-Hinton broth at 37 °C. Thirty microliters of the stock solutions were then added to sterile round bottom culture tubes (14 mL) to reach a final CFU of 1.0×10^6 in 3 mL total volume. Varied volumes of stock **1** (15 %, ACN) and AgNO$_3$ (10 mg/mL, H$_2$O) solutions were added to the prepared bacterial suspensions to achieve 0, 8, 4, and 2 μg/mL silver concentrations. AgNO$_3$ solutions were kept in the dark to prevent photodegradation. The final suspensions were incubated at 37 °C in a rotary mixer (40 rpm) for 18 h. Final sample suspensions were visually analyzed for bacterial growth and compared to control (containing water and ACN) and standard suspensions. All experiments were completed in triplicate.

2.8 Antibacterial assay

Effective therapeutic capacity of the Ag(ImD)$_{CMC}$ occlusive wound dressing (loaded with 1 % Ag) was assessed using a skin and soft tissue infection (SSTI) model inoculated with *E. coli*, reported previously by this group [14]. In short, 15 mL of a 5 % agar culture solution was first plated into a 100 mm sterile culture plate. To the solidified agar surface a batch of 10 mL of a 0.5 % agar solution inoculated with *E. coli* (final CFU 1.0×10^6 mL^{-1}) was then added to form the *soft* top layer. The plates were then incubated at 37 °C for 3 h to allow the top layer to slowly cool and solidify. After this incubation period, the prepared wound dressings were applied to the soft agar surface and allowed to incubate for 21 h. Finally, the dressings were removed and the bacterial loads of the application zones were compared to control samples that contained unloaded wound dressings. Leaching of **1** out of the silver-loaded wound dressing was observed by placing the SSTI plates on a UV table lamp at the end of the therapeutic exposure.

2.9 Bacterial cell culture

Strains of *E. coli* ATCC® 25922™ and *S. aureus* ATCC® 25923™ were employed in bacterial studies. Bacterial inoculants were taken from freeze-dried cultures and grown on Müller-Hinton agar surfaces and incubated for 24 h at 37 °C. From these plates single colony growths were taken to prepare the standard bacterial suspensions. Müller–Hinton broth solutions (5 mL) were inoculated with single colonies in 16 mm round bottom culture tubes and incubated for 6 h at 37 °C in a rotary mixer (40 rpm) to an OD_{600} between 0.6 and 0.9. From the standard suspensions, stock cultures were prepared to 1.0×10^8 CFU/mL and were employed for the MIC or SSTI assays as described above.

3 Results and discussion

3.1 Characterization of [Ag(ImD)$_2$]ClO$_4$

In our attempt to synthesize a trackable silver(I) complex for wound dressings, we have selected the highly fluorescent dye dansyl chloride as part of our ligand. The structure of the dansyl imidazole (ImD) ligand can be divided into two critical units. The first is the *silver-coordinating imi-dazole group*. This moiety was selected mainly on the basis of the extensive literature that identifies silver(I) imidazole complexes as potent antibacterial agents [15, 16]. These complexes effectively increase the bioavailability of Ag^+ leading to enhanced bactericidal action. The fluorescent dansyl group, the other part of the ligand frame, is often used as a protein tag and attaches to a wide variety of functional groups, including the imidazole group of histidine residues [17]. This fluorophore lacks antibacterial properties and acts solely as a visible maker of Ag^+ movement.

Addition of two equivalents of the argentophilic ImD ligand to AgClO$_4$ afforded [Ag(ImD)$_2$]ClO$_4$ (**1**), a cationic silver complex that exhibits excellent solubility in water. Shift of the ^{1}H NMR peaks corresponding to the protons of the imidazole moiety of ImD (from 8.27, 8.36, and 8.66 to 8.26, 8.46, and 8.70 ppm) confirmed coordination of the ligand to the metal center (Fig S4, Supporting Information). Single crystal X-ray diffraction analysis revealed a classic linear structure (N–Ag–N, 172.3(3)°) with the Ag^+ center ligated to two ImD ligands through the imidazole moiety (Fig. 1). The complex is relatively symmetric (Ag–N1 and Ag–N4 bond lengths of 2.120(7) and 2.109(7) Å, respectively) with the imidazole rings of the coordinating ligands lying within a single plane.

Electronic absorption spectrum of **1** exhibits no significant change in the absorption profile compared to the absorption spectrum of free ligand ImD with the λ_{max} (absorption band maximum) at 360 nm (Fig. 2). However, the extinction coefficient value at this wavelength increases from 2020 M^{-1} cm^{-1} to 7735 M^{-1} cm^{-1} upon ligation to the Ag^+ center. Similarly, minimal changes in the fluorescence excitation and emission profiles have been observed with the metal complex and the free ligand; only a small bathochromic shift in the emission band, from 480 to 500 nm, is noted upon excitation at 360 nm (Fig. 2).

Measurements on the photostability of **1**, studied by ^{1}H NMR spectroscopy, showed no apparent decomposition of the complex upon continuous exposure to ambient light for 24 h. In comparison, a purple-brown solid began forming in the standard AgNO$_3$ sample after only 1 h of equivalent light exposure. Further, the additional stability experiment performed

in MRD confirmed the stability of **1** in biological media because no evident change in the profile of the 500 nm excitation band (indicative of deligation) was observed over 24 h.

3.2 Therapeutic capacity of [Ag(ImD)$_2$]ClO$_4$

To establish the potential therapeutic capacity of **1**, minimal inhibitory concentration (MIC) experiments were completed against Gram-positive (*S. aureus*) and Gram-negative (*E. coli*) bacterial strains commonly known to inoculate wound sites [6]. Results of the MIC assays indicated that **1** displays MIC values of 2.3 and 4.7 μg/mL against *E. coli* and *S. aureus*, respectively. The observed MIC values are very much comparable to those reported for similar silver(I) complexes [15, 18, 19] and display significantly enhanced antibacterial capacity compared to many silver colloid and Ag-NP options [20, 21]. Enhanced efficacy of **1** against the Gram-negative *E. coli* is much in line with other silver(I) complexes and has been hypothe-sized to be a function of the cell structure of the bacterium that features a thinner peptidoglycan layer of the cell wall compared to Gram-positive bacteria.

3.3 Release of 1 from Ag(ImD)$_{CMC}$ pad

The Ag(ImD)$_{CMC}$ pads have been synthesized by a *one-pot* synthesis where a homogenous gel of NaCMC, PEG, **1** and water was poured into a sterile culture dish and dried to a desired consistency (calculated by % solvent loss equation). The final Ag(ImD)$_{CMC}$ pad exhibits a rubber-like texture that is rigid enough to be easily cut into any desired shape but slowly gels with the addition of water, a feature characteristic of hydrocolloid polymers (Fig. 3). The carboxymethyl cellulose frame was selected because it is a common wound dressing component that facilitates desloughing process at the wound bed (desloughing agent), assists in maintaining optimal wound moisture, and contains available anionic sites for electrostatic loading of the [Ag(ImD)$_2$]$^+$ cationic complex [22–24]. It should be noted that PEG was incorporated into the dressing components to help solubilize NaCMC into the water media. PEG is relatively bioinert and poses no apparent bactericidal action and for this reason can be considered an auxiliary component within the Ag(ImD)$_{CMC}$ pad [25].

Release of **1** from the pre-fabricated pre-weighed hydrocolloid gel discs into MRD solutions was monitored by fluorescence and absorption spectroscopy (Fig. 4). Analysis of the release profile collected over 24 h highlights an initial lag period in the first 8 h where the rate of release is relatively slow. However, after 8 h a linear release of **1** begins with a slope equating to leaching rate of 0.0027 ± 0.00045 μg/min (Fig. 4). The average weight of an Ag(ImD)$_{CMC}$ pad of 1 cm diameter is 75.6 mg, which equates to 64 μg of **1**. Based on this rate of release it can be calculated that under the defined experimental conditions, 5.2 μg of **1** are released after 24 h. Interestingly, decrease in the loading of **1** from 1 to 0.5 % in the CMC pads results in a decrease in the lag interval of **1** release from approximately 8 to 3 h with a leaching rate of 0.0068 ± 0.00012 μg/min. The increased rate of leaching with decreased loading of **1** presumably arises from variances in the Donnan potential of the systems [26]. While this property has more commonly been applied to explain movement across an impermeable membrane that separates liquid media with differing ionic species and net ion concentrations, it is applicable to hydrocolloid materials and ionic liquids that can act as phase boundaries impeding or controlling ion movement. Because cationic [Ag(ImD)$_2$]$^+$ units interact directly with the anionic carboxymethyl groups of the

hydrocolloid frame, the frame essentially resists change and movement of external ions into the network with higher loading. The 0.5 % Ag(ImD)$_{CMC}$ gel apparently reaches a dynamic state of ion movement much more quickly, as cationic species present in higher concentrations (relative to **1**) in the MRD solution move into the hydrocolloid frame and replace the cationic silver complex thus accelerating its movement out of the polymer network.

Qualitative leaching studies were conducted to observe the release of **1** from Ag(ImD)$_{CMC}$ disc onto an agar surface. The results revealed movement of **1** out of the hydrocolloid frame within the first 2 h of incubation. The transfer can be easily visualized by the linear increase in fluorescence intensity at the agar surface with time (Fig. 4). Taken together these findings establish *the tunability of therapeutic release of silver from the designed Ag(ImD)$_{CMC}$ pad, where leaching (delivery) rates and total dosages for defined time intervals can be controlled.* Such a feature could introduce the possibility of creating a wide spectrum of therapeutic dressings with leaching profiles tailored to control various levels and types of bioburden at wound sites.

3.4 Characterization of occlusive dressing

The complete occlusive dressing is comprised of three layers: (1) a hydrophobic Durapore ™ surgical layer, (2) Ag(ImD)$_{CMC}$ gel pad, and (3) sterile non-latex gauze (Fig. 5a). Because the Ag(ImD)$_{CMC}$ hydrocolloid pad can be prefabricated in any desired shape, occlusive dressing patches can be rapidly constructed in innumerable dimensions. To establish the therapeutic potential of the completed occlusive dressing, miniature prototypes of the dressings were prepared with 1 cm diameter Ag(ImD)$_{CMC}$ gel discs between 4 cm^2 Durapore™ tape and gauze squares. These prototypes were applied to a SSTI model inoculated with *E. coli*, which was shown to be more susceptible to **1** based on the calculated MIC values. *Incubation of the prototype dressing on the surface of the SSTI agar plate resulted in bacterial clearance and the kill zone overlays precisely with the visible fluorescence demarcation indicating delivery of* 1 (Fig. 5b). These results confirm the potential of the designed [Ag(ImD)$_2$]-loaded hydrocolloid-based dressing as a trackable Ag-delivery system. The ability to visually and spectroscopically monitor the therapeutic release can be exploited to optimize the rates of silver release from silver-based dressings and offer a level of detection for healthcare workers to visually observe therapeutic loading of silver to a wound site and identify the exhaustion of a dressing over time.

4 Conclusions

Silver-based therapeutics have long been utilized as antiseptic options given the oligodynamic effect of ionized silver. Resurgence in the use of this noble metal as an antibacterial agent is strong given the rapid onset of bacterial resistance toward traditional antibiotics. Although the application of topical silver agents and silver-loaded wound dressings in the control of bioburden at burn sites has been widely accepted, progress in the mode of delivery and sources of silver have remained quite limited. The current work highlights the synthesis of a silver(I) complex [Ag(ImD)$_2$]ClO$_4$ (**1**) that provides two levels of therapeutic improvement with the ligation of the fluorescent ImD group to a Ag$^+$ center.

The first level arises from the effective caging of the bioactive Ag^+ that ultimately yields significantly lower MIC values against Gram-positive and Gram-negative bacteria compared to many Ag-NP-based drugs reported previously. The second level is associated with a unique feature of *therapeutic trackability* where release of fluorescent $[Ag(ImD)_2]^+$ units from a carboxymethyl cellulose-based hydrocolloid carrier can be visualized by simply shining a UV source over the site of delivery (such as a handheld UV wand).

Supplementary Material

Refer to Web version on PubMed Central for supplementary material.

Acknowledgments

References

1. Atiyeh BS, Costagliola M, Kayek SN, Dibo SA. Effect of silver on burn wound infection control and healing: review of the literature. Burns. 2007; 33:139–48. [PubMed: 17137719]

2. Levy SB, Marshall B. Antibacterial resistance worldwide: causes, challenges, and responses. Nat Med. 2004; 10:S122–92. [PubMed: 15577930]

3. Arias CA, Murray BE. Antibiotic-resistant bugs in the 21st century: a clinical super-challenge. N Engl J Med. 2009; 360:439–43. [PubMed: 19179312]

4. Lansdown AB. Silver. I: its antibacterial properties and mechanism of action. J Wound Care. 2002; 11:125–30. [PubMed: 11998592]

5. Rai M, Yadav A, Gade A. Silver nanoparticles as a new generation of antimicrobials. Biotechnol Adv. 2009; 27:76–83. [PubMed: 18854209]

6. Klasen HJ. A historical review of the use of silver in the trea™ent of burns. II Renewed interest for silver. Burns. 2000; 26:131–8. [PubMed: 10716355]

7. Silver S, Phung LT, Silver G. Silver as biocide in burn and wound dressings and bacterial resistance to silver compounds. J Ind Microbiol Biotechnol. 2006; 33:627–34. [PubMed: 16761169]

8. Leaper DJ. Silver dressings: their role in wound management. Int Wound J. 2006; 3:282–94. [PubMed: 17199764]

9. Martin P. Wound healing-aiming for perfect skin regeneration. Science. 1997; 276:75–81. [PubMed: 9082989]

10. Diegelmann RF, Evans MC. Wound healing: an overview of acute, fibrotic and delayed healing. Front Biosci. 2004; 9:283–9. [PubMed: 14766366]

11. Velnar T, Mailey T, Smrkolj V. The wound healing process: an overview of the cellular and molecular mechanisms. J Int Med Res. 2009; 37:1528–42. [PubMed: 19930861]

12. Field CK, Kerstein MD. Overview of wound healing in moist environment. Am J Surg. 1994; 167:2S–6S. [PubMed: 8109679]

13. Winter GD, Scales JT. Effect of air drying and dressings on the surface of a wound. Nature. 1963; 197:91–2.

14. Heilman BJ, Halpenny GM, Mascharak PK. Synthesis and characterization and light-controlled antibiotic application of a composite material derived from polyurethane and silica xerogel with embedded photoactive manganese nitrosyl. J Biomed Mater Res B. 2011; 99B:328–37.

15. Rowan R, Tallon R, Sheahan AM, Curran R, McCann M, Kavangh K, Devereux M, McKee V. 'Silver bullets' in antimicrobial chemotherapy: synthesis, characterization and biological screening of some new Ag(I)-containing imidazole complexes. Polyhedron. 2006; 25:1771–8.

16. Melaiye A, Sun Z, Hindi K, Milsted A, Ely D, Reneker DH, Tessier CA, Youngs WJ. Silver(I)-imidazole cyclophane *gem*-diol complexes encapsulated by electrospun tecophilic nanofibers:

formation of nanosilver particles and antimicrobial activity. J Am Chem Soc. 2005; 127:2285–91. [PubMed: 15713108]

17. Gray WR. Dansyl chloride procedure. Method Enzymol. 1967; 11:139–51.

18. Nomiya K, Takahashi S, Noguchi R, Nemoto S, Takayama T, Oda M. Synthesis and characterization of water-soluble silver(i) complexes with L-histidine (H_2his) and (S)-(−)-2-pyrroli-done-5-carboxylic acid (H_2pyrrld) showing a wide spectrum of effective antibacterial and antifungal activities. Crystal structures of chiral helical polymers [Ag(Hhis)]$_n$ and {[Ag(Hpyrrld)]$_2$}$_n$ in the Solid State. Inorg Chem. 2000; 39:3301–11. [PubMed: 11196868]

19. Abu-Youssef MAM, Dey R, Gohar Y, Massoud AA, Öhrström MA, Lander V. Synthesis and structure of silver complexes with nicotinate-type ligands having antibacterial activities against clinically isolated antibiotic resistant pathogens. Inorg Chem. 2007; 46:5893–903. [PubMed: 17602550]

20. Chernousova S, Epple M. Silver as antibacterial agent: ion, nanoparticle, and metal. Angew Chem Int Ed. 2013; 52:1636–53.

21. Fayaz AM, Balaji K, Gitilal M, Yadav R, Kalaichelvan PT, Venketsan R. Biogenic synthesis of silver nanoparticles and their synergistic effect with anibiotics: a study against Gram-positive and Gram-negative bacteria. Nanomed-Nanotechnol. 2010; 6:103–9.

22. Czaja W, Krystynowicz A, Beilecki S, Brown RM. Microbial cellulose-natural power to heal wounds. Biomaterials. 2006; 27:145–51. [PubMed: 16099034]

23. Ramli NA, Wong TW. Sodium carboxymethylcellulose scaffolds and their physicochemical effects on partial thickness wound healing. Int J Pharm. 2011; 403:73–82. [PubMed: 20974238]

24. Hoffman AS. Hydrogels for biomedical applications. Adv Drug Deliv Rev. 2002; 54:3–12. [PubMed: 11755703]

25. Peppas NA, Torres-Lugo M, Lowman AM. Poly(ethylene glycol)-containing hydrogels in drug delivery. J Control Release. 1999; 62:81–7. [PubMed: 10518639]

26. Sannino A, Demitri C, Madaghiele M. Biodegradable cellulose-based hydrogels: design and applications. Materials. 2009; 2:353–73.
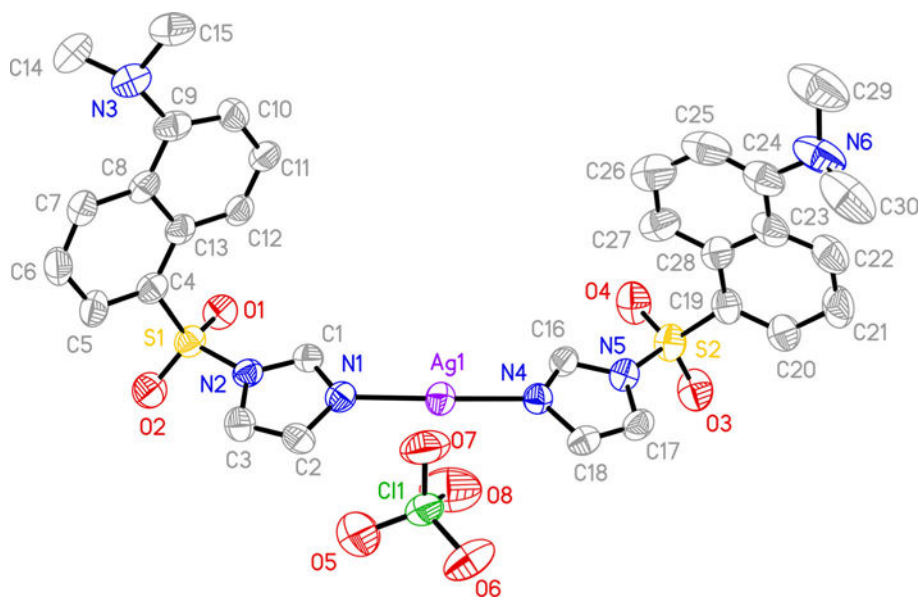
Fig. 1.
Thermal ellipsoid plot of [Ag(ImD)$_2$]ClO$_4$ (**1**) shown with 50 % probability ellipsoids (H atoms are omitted for clarity)
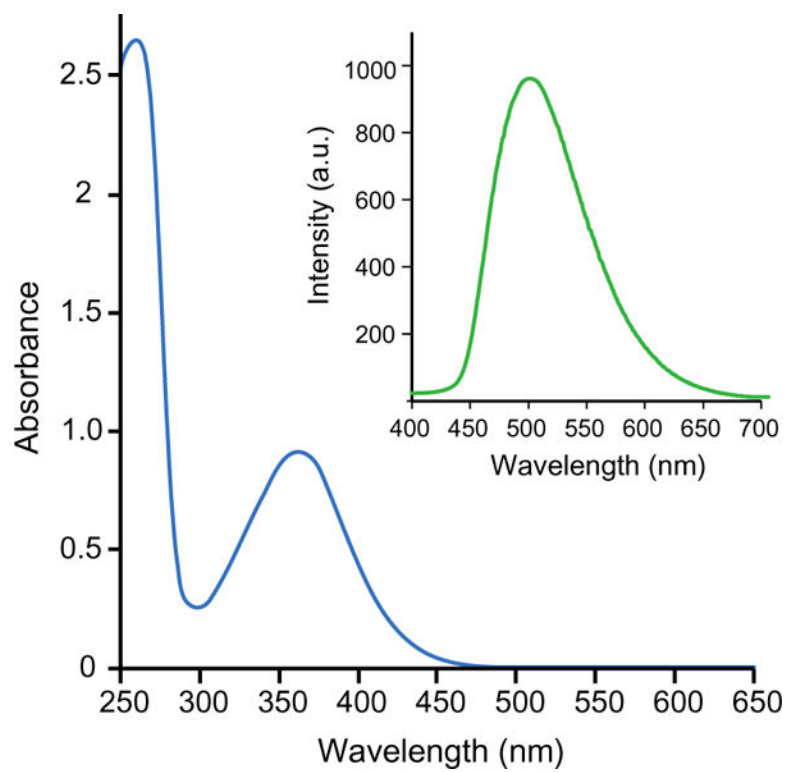
Fig. 2.
Electronic absorption spectrum of 130 μM of **1** in ACN. *Inset* Emission spectrum of **1** with 360 nm excitation
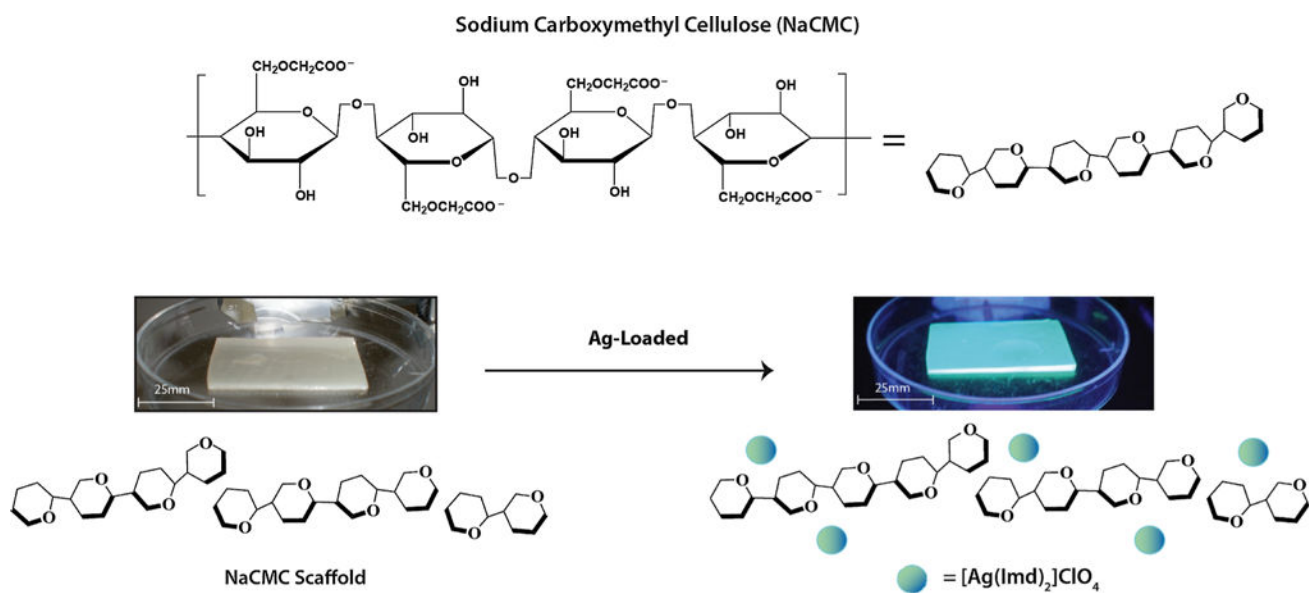
Fig. 3.
Schematic representation of loaded and unloaded carboxymethyl cellulose (CMC) pads. The *left* image shows an unloaded non-fluorescent CMC pad and the *right* image presents a loaded Ag(ImD)$_{CMC}$ pad. The images highlight the pliable rubber-like consistency of the CMC-based pads

Fig. 4.
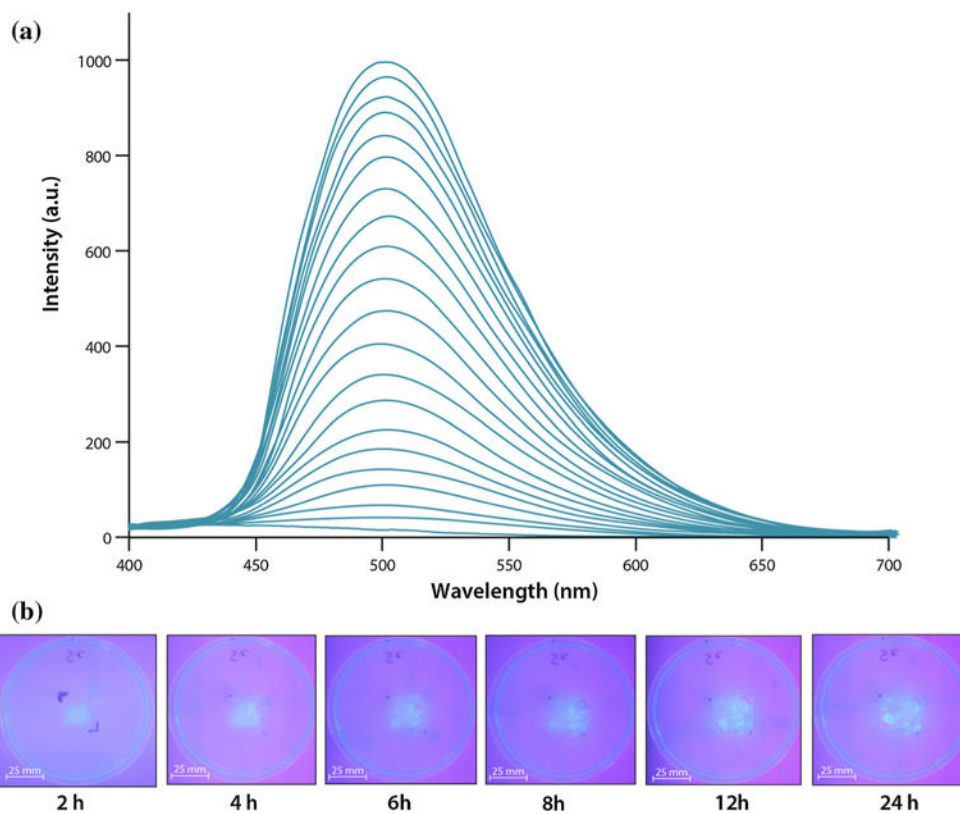**a** Fluorescent spectrum observed over 24 h of leaching of **1** from Ag(ImD)$_{CMC}$ disc in MRD solution. Spectral traces show the general increase in absorbance, indicating release of **1** into the solution. **b** Solid-phase leaching of **1** into agar layer
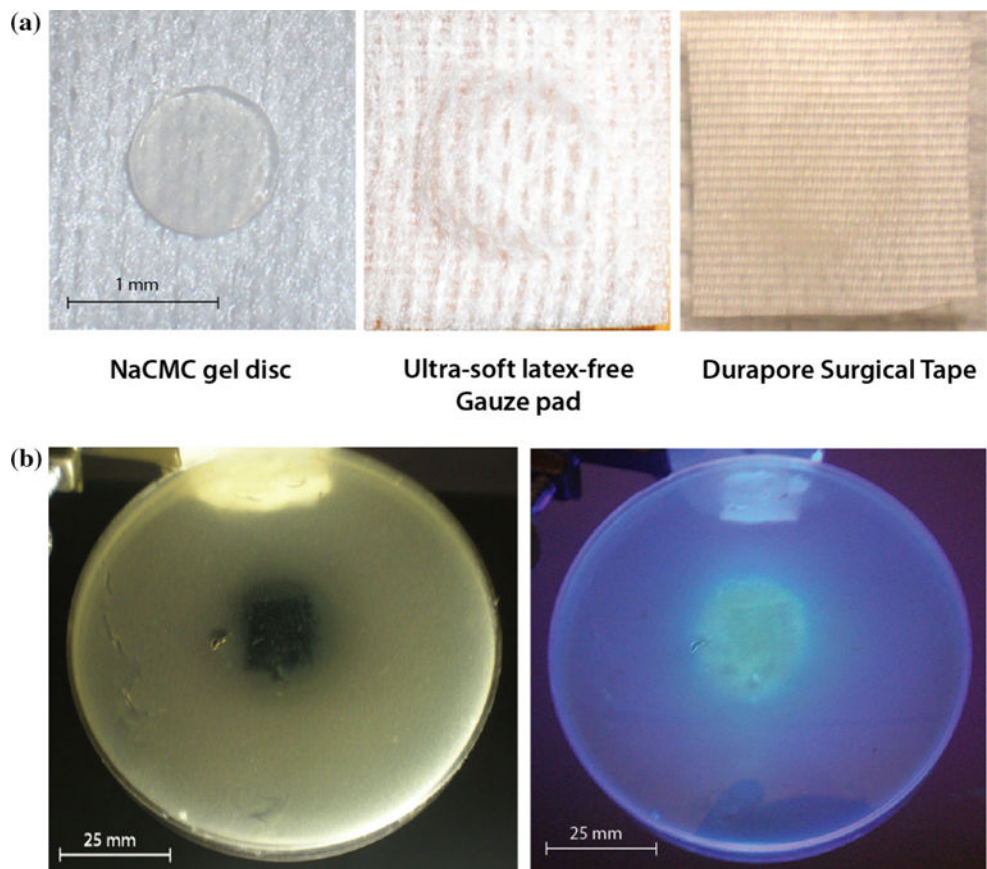
Fig. 5.
a Complete occlusive dressing prototype shown in layers with the Ag(ImD)$_{CMC}$ disc shown at the far *left*, latex-free gauze pad (surface that would directly interact with the surface of a wound) in the middle, and the top protective Durapore layer on *right*. **b** SSTI agar plate observed after 21 h exposure to a Ag(ImD)$_{CMC}$ (1 % Ag loaded) dressing. The image on the *left* highlights the bacterial clearance that overlays with the loading of fluorescent **1** on the kill zone shown on the *right*